HHS Public Access

Author manuscript

SLAS Discov. Author manuscript; available in PMC 2024 July 25.

Published in final edited form as:

SLAS Discov. 2020 March ; 25(3): 265–276. doi:10.1177/2472555219880194.

A 3D heterotypic multicellular tumor spheroid assay platform to discriminate drug effects on stroma versus cancer cells

Zoe Weydert[1,§], **Madhu Lal-Nag**[2,§], **Lesley Mathews-Greiner**[2], **Christoph Thiel**[3], **Henrik Cordes**[3], **Lars Küpfer**[3], **Patrick Guye**[1], **Jens M. Kelm**[1,4,*], **Marc Ferrer**[2,*]

[1]InSphero AG, Wagistrasse 27A, 8952 Schlieren, Switzerland

[2]NIH/NCATS, 9800 Medical Center Drive, Rockville, MD 20854 USA

[3]PreComb Therapeutics AG, Einsiedlerstrasse 32, 8820 Wädenswil, Switzerland

[4]Institute of Applied Microbiology (iAMB), Aachen Biology and Biotechnology (ABBt), RWTH Aachen University, Worringerweg 1, 52074 Aachen, Germany

Abstract

Three-dimensional cell culture models are thought to mimic the physiological and pharmacological properties of tissues *in vivo* more accurately than two dimensional cultures on plastic dishes. For the development of cancer therapies, 3D spheroid models are being developed to reflect the complex histology and physiology of primary tumors with the hopes that drugs responses will be more similar to those obtained *in vivo*. The effect of additional cell types in tumors, such as stromal cells, and the resulting heterotypic cell-cell crosstalk can be investigated in these heterotypic 3D cell cultures. Here, a high throughput screening compatible drug testing platform based on 3D multicellular spheroid models is described which enables the parallel assessment of toxicity on stroma cells and efficacy on cancer cells by drug candidates. These heterotypic microtissue tumor models incorporate NIH3T3 fibroblasts as stromal cells which are engineered with a reporter gene encoding secreted NanoLUC luciferase. By tracking NanoLUC signal on the media over time, a time-related measurement of the cytotoxic effects of drugs on stromal over the cancer cells was possible. An *in vitro* therapeutic index parameter is proposed to help distinguish and classify those compounds with broad cytotoxic effects versus those that are more selective at targeting cancer cells.

Keywords

3D heterotypic spheroids; stroma; therapeutic index

INTRODUCTION

Drug discovery is a process that requires large and high-risk investments in scientific research and pre-clinical and clinical development [1–3]. It is therefore crucial to have

*Corresponding authors: Marc Ferrer, PhD, NIH/NCATS, 9800 Medical Center Drive, Rockville, MD 20854 USA, Jens M. Kelm, PhD, PreComb Therapeutics AG, Einsiedlerstrasse 32, 8820 Wädenswil, Switzerland.

§equal contributors

compound activity data that accurately predictive effects in humans sooner in the drug development process. Traditionally, drug discovery process for anti-cancer agents has relied on *in vitro* cell proliferation models in which cancer cell lines are cultured as monolayers adhered on plastic surfaces [4,5]. However, it is becoming more evident that such two-dimensional (2D) cell culture models, although very amenable to high throughput screening (HTS) of large collections of compounds, do not reproduce the physiological complexity of a tumor *in vivo*. As a consequence, compounds having promising pharmacological effects on 2D cultures often fail to produce an effect in a clinical setting [5,6,7]. As a consequence, three-dimensional (3D) cell assay systems are being explored to create more clinically relevant models of tumors for drug development [4,5,8–11]. In contrast to 2D cell cultures, 3D culture conditions can better mimic the multicellular interactions within the tumor and with the microenvironment of tumors, which has significant impact on the cellular behavior and pharmacological responses [12–16]. In this regard, inclusion of stromal cells in heterotypic cell models have been shown to stimulate the proliferation of cancer cells and affects their inter-cellular signaling and gene expression [5,17–19]. Therefore, the use of a heterotypic 3D model may offer substantial advantages for investigating the effect of potential anti-cancer agents.

The overall goal of this work was to develop a model system which allows for the discrimination of cell viability patterns of two cell types within a heterotypic microtissue tumor model, and to classify the cytotoxic effects of compounds tested on each cell type in the context of the entire microtissue system. The expected benefit of such a discrimination in the specific case of cancer and stromal cells *in vitro* is to predict the therapeutic window of a drug *in vivo*. This 3D multicellular heterotypic spheroid model is amenable to high throughput (HTS) screening and enables the parallel assessment of drug efficacy on cancer cells and unspecific cytotoxicity on tumor integrated stroma cells of drug candidates. Homo- and heterotypic ovarian and pancreatic microtissue models were developed and used for the screening of a focused set of anti-cancer compounds targeting different mechanisms considered the hallmarks of cancer[20]. One pancreatic and two ovarian cell lines were used for the development of the microtissue tumor models. Although pancreatic and ovarian cancers are relatively rare diseases, pancreatic cancer is the fourth leading cause of cancer-related mortality, and ovarian cancer is the most common cause for gynecological cancer death [19,21]. The introduction of a secreted NanoLUC luciferase reporter gene into a fibroblast stroma cell allowed direct discrimination of cytotoxic effects between these non-proliferative cells and the proliferating cancer cells within a heterotypic tumor spheroid. An *in vitro* therapeutic index parameter resulting from a 3D anti-cancer drug screening is proposed to help distinguish and classify those compounds with broad cytotoxic effects versus those that are more selective in targeting cancer cells.

MATERIALS AND METHODS

General Cell Culture.

The HEY cell line is a human ovarian carcinoma cell line and was derived from a xenografted tumor (HX-62). The ovarian cancer xenograft was originally grown from a peritoneal deposit of a moderately differentiated papillary cystadenocarcinoma of the ovary.

The HEY-GFP cell line was obtained from Dr. Ernst Lengyel, University of Chicago. The HEY-GFP cells were cultivated in RPMI 1640 medium with 10 % FBS, 1 % Pen/Strep and 25 mM Hepes. The SKOV-3 cell line was obtained from ATCC and is a human ovarian cancer cell line that was established from a 64 years old female patient, suffering from ovarian adenocarcinoma. The SKOV-3 cells were cultivated in DMEM medium with 10 % FBS, 1 % Pen/Strep, 1 % NEAA and 25 mM Hepes. The PANC-1 cell line was obtained from ATCC and is a human pancreatic cancer cell line established from a 56 years old male patient, suffering from pancreatic epithelioid carcinoma. The PANC-1 cells were cultivated in DMEM medium with 10 % FBS, 1 % Pen/Strep and 25 mM Hepes. The NIH3T3 cell line is a mouse embryonic fibroblast. The NIH3T3 cells were cultivated in DMEM medium with 10 % FBS, 1 % Pen/Strep and 25 mM Hepes.

Microtissue production process.

After expanding the cells, they were detached and the cell suspension with the desired cell density (HEY-GFP 100 cells/drop, SKOV3 200 cells/drop, PANC1 200 cells/drop and NIH 3T3 (5000 cells/drop) was prepared. To produce heterotypic microtissue models, a cell suspension containing both fibroblasts and the respective cancer cells was prepared in DMEM medium. The cell suspension was seeded into the GravityPLUS™ plate (InSphero AG, Schlieren, Switzerland) by pipetting 40 µl suspension per well. For aggregating the cells into microtissues, the loaded plate was placed into an incubator for 72 hours. For longtime cultivation and compound treatments the microtissues were transferred three days after seeding from the GravityPLUS™ into the GravityTRAP™ (InSphero AG) plate. A medium exchange was performed twice a week to prevent the microtumors from nutrient starvation. To observe the morphology of the microtissues over time, bright field (BF) images were taken on a regular basis (Zeiss Axiovert 25, 5x).

Histological analysis.

Microtissues were fixated and embedded in agarose. The microtissues were collected from the GravityTRAP™ plate into an Eppendorf tube and washed with PBS. After washing, the microtissues were fixated by adding PFA for at least 1hr at RT. The PFA was then removed and 600 µl of boiled agarose solution was added for embedding. After solidification of the agarose plug, 500 µl PBS was added into the tube. The subsequent paraffin embedding, cutting of paraffin blocks and the IHC staining itself was performed on order by an external company (Sophistolab).

Transfection of the NIH3T3 fibroblasts.

In order to discriminate stromal cells from cancer cells in heterotypic microtissue models, a reporter gene was introduced into the fibroblasts in order to secrete NanoLUC® luciferase. Transfection of the NIH3T3 fibroblasts by Nucleofection in order to secrete NanoLUC® luciferase (pNL1.3CMV[secNluc] luciferase reporter vector, Promega) was performed according to Lonza's manual Amaxa™ 4D-Nucleofector™ Protocol for NIH/3T3 (Lonza Cologne GmbH, Cologne, Germany) using a Single Nucleocuvette™ (100 µl). The cells were trypsinized and an aliquot of 10^6 cells was resuspended in 100 µl 4DNucleofector™ Solution (Lonza Cologne GmbH). 1 µg of pNL1.3CMV [secNluc] luciferase reporter vector was added, and the suspension was transferred into a Nucleocuvette™. The Nucleocuvette™

was placed into the 4D-Nucleofector™ X Unit. The cells were transfected with program EN-158. After transfection the cells were plated in cell culture medium into a T-flask. For separation of the dead cells, the flask was incubated overnight, and vital cells were allowed to adhere to the bottom. The vital cells were subsequently used for the microtissue production process.

Drug testing.

Thirty-eight compounds covering major cancer pathways were selected for testing in the different cancer spheroid models and were purchased commercially from different sources. The 38 compounds included 26 anti-cancer agents, two antibiotics, two cardiac glycosides, an anti-psychotic and an antidepressant drug, an antiarrhythmic and an anticonvulsant agent, an epithelial sodium channel blocker, a L-DOPA inhibitor, an androgen receptor antagonist, as well as a drug acting on chemokine receptors. Table S1 shows the list of the compounds and their respective primary mechanism of action. In addition, the table provides a potential categorization according to the respective effects of the compounds on one or more cancer hallmarks. All 38 compounds were tested on the ovarian HEY homotypic and HEY/NIH heterotypic microtissues. 20 compounds were tested on the ovarian SKOV/NIH and pancreatic PANC/NIH heterotypic microtissues. The treatment was started after transferring microtissues into the assay plate, re-dosing of the microtissues was performed at day 3 and 5. Compounds were tested within a concentration range of 2 pM – 20 μM (11 doses, 1:5 dilution series). The vehicle control group consisted of microtissues treated with 1 % DMSO in microtissue maintenance medium. A 1:5 dilutions series of the compounds was prepared in a separate V-bottom plate with DMSO as diluent. To reach a final concentration of 1 % DMSO a second dilution step was performed with microtissue maintenance medium as diluent.

Measurement of Microtissue Size over time.

To monitor microtissue size and morphology over time, the Dainippon SCREEN Cell3iMager was used. 96-well plates were scanned at treatment days 3, 5 and 7. The integrated analysis software enabled automated measuring of the microtissue size, including accurate discrimination of microtissues and cell debris which might occur after compound treatment.

Nano-Glo® Luciferase Assay.

To discriminate fibroblasts from cancer cells in the co-culture models, the fibroblasts were transfected with a reporter gene in order to secrete NanoLUC luciferase. Within a screening run the secreted NanoLUC® luciferase was measured 3, 5 and 7 days after the treatment started. The Nano-Glo® Luciferase Assay was performed according to Promega's manual Nano-Glo® Luciferase Assay System (Promega).

CellTiter-Glo® Luminescent Cell Viability Assay.

As a biochemical endpoint of a screening run at treatment day 7, the cell viability of the microtissues was detected by measuring the ATP content. The procedure for the CellTiter-Glo® 3D Cell Viability Assay was done as follows: The complete culture medium

was aspirated manually; CellTiter Glo® 3D Reagent was mixed 1:1 with microtissue maintenance medium and 40 µl of the diluted reagent was added to the microtissues and mixed. Microtissues and supernatant were transferred into a 96-well Half-Area white assay plate (Corning Cat 07–200-326). The assay plate was wrapped in aluminum foil and incubated for 20 minutes at room temperature while shaking horizontally. Luminescence was measured with the Tecan M200Pro. For analysis of the data the values from treated microtissues were normalized to the vehicle control.

Data analysis and visualization.

For the generation of dose-response curves and corresponding IC50 values, the data obtained from size measurements, NanoLUC assays and ATP assays were normalized to the vehicle control. The normalized data was processed using the GraphPad Prism® 6 Software. The program uses the subsequent formula for fitting a sigmoidal dose-response curve: Y = ((Y_top))/(1 + 〖10〗 ^((Log IC_50 – X)* HillSlope)); Ytop is the Y value at the top plateau. The Hill Slope variable, also called the Hill Slope coefficient, describes the steepness of the curve. Visualizations which were set up via TIBCO Spotfire software.

Multi-parametric compound classification.

The multi parameter classification aims to harmonize data features derived from different tumor micro tissues with diverging scales and ranges. In this study, data was generated for a set of 20 drugs from the NCTAS library describing the potency, efficacy, acute toxicity and chronic toxicity of each drug as well as the impact of a drug on tumor growth. For each tumor micro tissue (HEY/NIH, SKOV-3/NIH, and PANC/NIH) ranked lists of different feature combinations were generated including a 3 feature combination of potency, efficacy and tumor growth was well as a five feature combination of potency, efficacy, tumor growth, acute toxicity and chronic toxicity. For both lists, the rank of a drug is dependent on the biological impact of each feature i.e. a small IC_{50} ATP value indicates a high potency of a drug and is therefore ranked lower (better). In this regard, a high efficacy, low acute and chronic toxicity as well as a strong inhibition in tumor growth result in lower ranks. The final rank of a drug in each tumor tissue list (i) is determined by the equal weight rank ($\bar{R}_i$) over all considered feature ranks ($r_{i,n}$) (n=3 and n=5).

$$\bar{R}_i = \sum_1^n r_{i,n}/n$$

A comparison over all drugs between the different tumor lists is enabled with the Spearman rank correlation ranging from 0 to 1, were zero indicates not correlation and 1 a perfect correlation. To compare the efficacy of a drug throughout all different tumor micro tissues, the equal weight ranks from all tumor types were reranked between 1 and # of compounds. The average rank of all tumor tissues determines the overall rank of a drug.

RESULTS

The assessment of the morphological and growth properties of several heterotypic tumor microtissues was performed to define assay parameters for their pharmacological profiling.

Three heterotypic microtissue models were established, all including a cancer cell line and NIH3T3 fibroblasts, as stromal cells: (i) ovarian cancer co-cultures with HEY-GFP tumor cells, referred to as HEY/NIH microtissues; (ii) ovarian cancer co-culture systems with SKOV-3 as tumor cells, referred to as SKOV/NIH microtissues; and (iii) a pancreatic cancer co-culture system with PANC-1 as tumor cells, referred to as PANC1/NIH microtissues. The aggregation of the respective cells in hanging drops resulted in microtissue formation within 3 days, observed by bright field microscopy. After microtissue formation, microtissues were either harvested for histological analysis or transferred into a non-adhesive spheroid-specific 96-well plate for long-term culture. Growth profiles were obtained by measuring size over time using bright field microscope. All three models displayed fast growth characteristics, and at 10 days, HEY/NIH being 6x and SKOV/NIH and Panc-1/NIH being 3x larger than the size of the microtissues at 3 days (Figure 1 A–F). Due to the fast growth kinetics of HEY/NIH microtissues, tissues were initiated with 50% fewer cancer cells in the starting cell mixture. To investigate cell viability over time, the ATP content was measured regularly over a culture period of up to 13 days (Figure 1 D–F). The increase in size of the microtissues seen by bright field microscopy correlated with a parallel increase in ATP levels in the tissues, as measure by the reagent CellTiterGlo™, indicating a corresponding increase in number of viable cells in the microtissue.

Characterization of internal architecture of the microtissues was done by histological sectioning and IHC staining. After 3, 6 and 11 days of culture, IHC analyses of the co-culture microtissues were performed (Figure 1 G–I). H&E staining of heterotypic spheres allowed for a discrimination between cancer and stromal cells due to their different morphology and spheroid location. H&E staining of co-culture microtissues confirmed of a viable microtissue although, and in contrast to homotypic microtissues (Figure S1), the formation of a necrotic area in the center of the spheres was observed after 11 days of culture. IHC staining of with EGFR and Ki67 allowed to clearly distinguish the cellular plasticity of these heterotypic microtissues during cultivation, in which initially, a central core of non-proliferating fibroblasts is quickly formed with proliferating cancer cells attached to the periphery, and then, with time, the tumor cells grow and start migrating to the inside of the microtissue. There was a slight upregulation of EGFR in the cancer cells of heterotypic spheres, recognizable by being more expressed in co-culture compared to homotypic microtissues (Figure 1G–I and Figure S1). HEY/NIH, SKOV/NIH and PANC/NIH microtissues equally showed a high expression of these proteins. Upregulation of collagen IV could be detected when HEY cells were co-cultivated with fibroblasts, as compared to homotypic microtissues (Figure S1D, E) for HEY and HEY/NIH, data not shown for SKOV/NIH and PANC/NIH. Considering the generally weak IHC staining of collagen IV, the expression of collagen IV could be displayed in both, HEY/NIH and PANC/NIH microtissue models, whereas collagen IV expression within SKOV/NIH spheres could not be shown clearly underlining cancer cell-specific interactions with fibroblasts. In conclusion, the growth and morphological data show a picture of assembly of microtissues in which the fibroblasts formed a non-proliferating core into which the cancer proliferate to make the sphere larger, increase in ATP levels likely reflects the increase in mostly the number of cancer cells rather than fibroblasts. Based on the growth kinetics, NanoLuc® secretion stability with time (Figure S2), and histological appearance, the treatment time

was set to 7 days for pharmacological profiling. Over this time period, there was robust growth of the tissues without observing significant necrosis in the core, and robust stable of NanoLuc® detect cytotoxicity on non-tumor cells.

The effects of a set of drugs with different mechanism of action (see Table S1) were first tested on the different cellular models of ovarian cancer using the HEY cells grown in a monolayer, homotypic microtissues and heterotypic HEY/NIH microtissues. The effects of the drug on the growth of the cells in each assay system was assessed by measuring ATP content after a 2-day treatment period for the monolayer cultures model; and microtissue size at 3-, 5- and 7-days by brightfield imaging and ATP after 7-day treatment for the 3D microtissue cultures. Figure 2A shows a heat map of the % cell viability at the maximum dose of compound tested (% maximal response) which is a measure of compound efficacy, for each assay condition. Most of the 20 compounds tested were highly efficacious in the ATP monolayer assay, except for PNU-74654. The measured % maximal responses by both ATP measurement at day 7 and tissue size at day 7, revealed a similar responsiveness to the drug treatments of homo- and heterotypic microtissues, with a tendency for homotypic microtissues being more sensitive to the compounds. However, there is also a clear tendency that the temporal effects of the drugs on the size of heterotypic microtissues is less pronounced as compared to homotypic microtissues, and in general, the time that it takes to see an effect is longer for heterotypic microtissues. For microtissues, of the 20 compounds, at day 7, most were efficacious in both assay readouts and tissues, except for PNU-74654, VU0483488-1, and GM-6001, especially in the heterotypic tissue. Correlation plots of % maximal responses (Figure 2B, C) confirms that efficacy of the compounds correlates between homo- and heterotypic microtissues; however, although there is a good correlation, compounds appear to be more efficacious for the homotypic microtissues by both readouts (Figure 2B, C). A good correlation was also observed when evaluating the potencies (AC_{50} values) of the compounds (Figure 2D, E and Table S2) comparing heterotypic and homotypic microtissues, both by ATP and tissue size measurements. The evaluation of the maximal responses (efficacy) and AC_{50} (potency) data indicated that heterotypic microtissues show a decrease in efficacy to compounds compared with homotypic microtissues, although the potencies of the compounds remain very similar between the two cellular systems.

To assess differences in the pharmacological responses of the different cancer types in the context of heterotypic microtissues, the efficacies and potencies of the 20 compounds were evaluated in the two ovarian (HEY/NIH, SKOV/NIH) and the pancreatic (PANC/NIH) heterotypic microtissue models. The % maximal responses based on ATP measurements after 7 days revealed similar efficacies of the tested drugs in all cancer heterotypic macrotissues (Figure 3A). The % maximal responses based on tissue size measurements at different time points showed that the efficacy of the compounds in all heterotypic tissue models generally increased with treatment time and by day 7 most of the compounds were efficacious in all cancer microtissues (Figure 3). A comparison of AC_{50} values of the different heterotypic tissue systems showed that in general, the potencies of the compounds correlated between the same assay readout (ATP) across different cancer type (Figure 3B–D), and same cancer types across different readout (Figure 3E–G). Only for SKOV3 microtissues, drugs appeared to be less sensitive (>5-fold AC_{50} ratio) by tissue size than

ATP measurements (Table S3). Several compounds including Torin-1, TAK-733, SR-3066, Dasatanib, and Carfilzomib had AC_{50}< 100nM in all heterotypic cancer tissue types, as measured by ATP at 7 days. The NF-kappaB inhibitor Bardoxolone methyl is an example of a compounds that was very potent for SKOV3 microtissues with a >1000-fold selectivity over the other cancer microtissues by ATP 7 days readout. These results indicate that different histological subtypes of a particular cancer can have an influence on the responses to a drug. When measuring the size of the different cancer heterotypic spheroids, the efficacy of the compounds reported as the % maximal response show a trend of increasing at the later 7 day after treatment, for the three cancer tissues. However, it is clear that for HEY/NIH3T3 tissues, the efficacy of the compounds was much greater at the 3 days' time point, than for the other two cancer heterotypic microtissues. When comparing the potency of the compounds as measured by the log AC_{50}, in general there was very good correlation between cancer type microtissues when using the ATP readout at 7 days. When comparing readouts in a cancer tissue type, although in general there was a good correlation between the potencies by ATP and tissue size readouts, for the three cancer microtissues, for the SKOV3 and PANC1, the AC_{50}s were about 10-fold more potent in the ATP that for the tissue size readout, while for the HEY, the AC_{50}s were very similar. In conclusion, both the efficacy and potency data across heterotypic tissues show very similar drug effects regardless of the different cancer types at the 7 days, while at 3 and 5 days, the drug effect on size was much more effective in HEY heterotypic tissues than PANC1 and SKOV3 tissues, which were more resistant.

The reduction of severe side effects which are commonly associated with traditional chemotherapeutic agents is one of the main drivers for developing cancer-specific targeted therapeutics. In order to identify toxic side effects of the tested compounds on stromal cells, luminescence signal from secreted NanoLUC luciferase of the transiently transfected stromal fibroblasts was measured from the heterotypic tumor microtissues, over treatment time. The heat map in Figure 4A illustrates the % maximal responses calculated on the basis of secreted NanoLUC data over time compared to tissue size measurements at the same times. The NanoLUC activity values at the respective measurement days of the dosed conditions were normalized to the NanoLUC activity of the untreated control. As a result, 100 % NanoLUC signal was representing 100 % stromal viability. As observed when measuring size of the tissues, the efficacy of the drugs tested increases with the length of treatment and by day 7, most of them reduced NanoLuc signal by >50%. Some of the compounds, like Romidepsin, an HADC inhibitor, have a strong effect on the NanoLuc but no effect on tumor size at day 3, which suggests transcription downregulation of NanoLuc expression by epigenetics modulation, and not necessarily cytotoxic effects on the fibroblasts, thus highlighting one of the caveats of our approach. Another set of interesting compounds are those that reduce tumor size early in the treatment without affecting NanoLuc signal, including Dasatanib, TAK-733, WAY-600 for HEY/NIH3T3, although none such compounds were observed to have an effect for SKOV3/NIH3T3 and PANC1/NIH3T3 tissues, at any of the time points. This data illustrates that besides the overall trend of increase efficacy with time, both by NanoLuc and tissue size, it is clear that the time-dependent increase in efficacy for each compound is cancer tissue dependent. These varying effects of the compound on the efficacy by NanoLuc and ATP and tissue

size readouts is also observed in correlation plots (Figure 4B). The heat map in Figure 4C illustrates the logAC_{50} for those compounds that produced enough of an efficacious response to be able to fit a dose response to calculate an AC_{50} value (a dark cell box indicate that a curve fit was not possible because of very small efficacy). Mirroring the increased time-dependent efficacy, compounds appear more potent at day 7 also, by measuring the NanoLuc signal, and in general, there is a good correlation between the potencies of the compounds for all the cancer tissues. There are compounds like Torin 2, TAK-433 and Romidepsin that are very potent compounds at day 7 by both measures and across all cancer tissues, and other compounds like Bardoxolone methyl which is very potent only for SKOV3 tissues, as was discussed above.

To model a therapeutic window between cytotoxic effects on cancer cells over stromal cells, we calculated a ratio between AC_{50} values based on NanoLUC activity over AC_{50} values based on ATP activity at day 7 (Table S4). We calculated two different therapeutic windows modeled based on pharmaco- and toxicokinetic concept and taking advantage of our temporal readouts: NanoLUC data at day 3 after treatment represented acute toxicity of the compounds, whereas NanoLUC data at day 7 after treatment represented chronic toxicity. The calculated therapeutic windows for HEY/NIH spheroids are shown in Table 1, and for SKOV/NIH and PANC/NIH microtissues are listed in Table S4 For some compounds for which no significant effect was observed on the fibroblasts, an AC_{50} value could not be calculated, and the therapeutic window of the respective compound was assumed to be infinite. For PANC1/NIH tissues, at day 3, none of the compounds had acute toxic effect except for Torin-2. However, even Torin-2, the only compound for which an AC_{50} value with regard to fibroblast toxicity was computable, showed a very broad therapeutic window with the ratio of adverse to therapeutic effect being 5,524-fold. In contrast, the fibroblasts within the SKOV/NIH microtissues seemed to be more sensitive to the compounds at day 3. In particular, Romidepsin significantly lowered the viability of the stromal cells within 3 days of treatment. An analysis of the therapeutic windows for SKOV/NIH microtissues at day 7 showed that two compounds, Dasatinib and WAY-600, which had medium to high therapeutic effects, did not have chronic toxicities with respect to fibroblasts. In PANC/NIH microtissues, Torin-2 showed a broad therapeutic window even after 7 days of treatment. This suggests that those compounds specifically targeted the cancer cells. Similar to what was observed in SKOV and PANC microtissues, most of the compounds did not exhibit acute toxicity for stromal cells in HEY/NIH spheroids (Table 1). Romidepsin, which had a narrow therapeutic window at day 3 in SKOV/NIH microtissues, did not seem to have toxic effects on fibroblasts at day 3 in HEY/NIH microtissues. However, after 7 days of treatment, the adverse effects of Romidepsin outweighed the therapeutic effects in HEY/NIH microtissues. As opposed to Romidepsin, Dasatinib which is a very potent compound measured in terms of ATP content, showed a large therapeutic window even after 7 days of microtissue treatment in both ovarian cancer models. The variations in therapeutic windows between the different microtissue models may be caused by different therapeutic effects of the compounds on the one hand, or by variations in adverse effects on the other hand. To compare the chronic toxicity with respect to stromal cells in the different heterotypic microtissues, correlation plots with NanoLUC data at day 7 were generated (Figure 4B). The chronic toxic effects of the compounds on fibroblasts were comparable under the

different model systems. Interestingly, within the group of compounds which generally exhibited a high toxicity, fibroblasts within PANC/NIH and SKOV/NIH microtissues were more sensitive compared to fibroblasts within HEY/NIH microtissues. Vice versa, within the group of compounds with generally lower toxicities, the compounds showed stronger effects in HEY/NIH fibroblasts compared with SKOV/NIH and PANC/NIH stromal cells.

To further define compound criteria to help prioritize compounds based on both high cytotoxicity effects on cancer cells and reduce toxicity on stromal cells, the compounds were ranked with respect to their efficacy, potency, acute toxicity, chronic toxicity and their effects on tumor size over time. For each category the 10 outstanding compounds are shown (Table 2, Table S5, Table S6). Ranked as best in terms of efficacy were the compounds which showed the lowest relative max responses based on ATP data. Best in terms of potency were the compounds which showed the lowest IC_{50} values based on ATP data. Best in acute toxicity were compounds which showed the highest NanoLUC signal at day 3 after treatment. Best in terms of chronic toxicity were compounds which showed the highest NanoLUC signal at day 7 after treatment. In the specific case of compounds which showed infinite values, the compounds were ranked according to their respective IC_{50} values based on ATP data. Best in terms of effect on tumor size over time were the compounds which resulted in lowest tumor growth over time. Table S4 shows the compound classification for HEY/NIH tumor spheroids.

Within this ranking the four compounds Dasatinib, TAK-733, Sepantronium bromide and Carfilzomib may be highlighted. Dasatinib is listed in all categories, except for efficacy, where it was ranked 14th out of 38. The same applies to TAK-733, which was ranked 17th in terms of efficacy. Sepantronium bromide which showed broad therapeutic windows for both acute and chronic toxicity, exhibited a high efficacy and had a high influence on tumor growth over time. It was ranked 13th in terms of potency with an IC_{50} value of 0.279 μM. Carfilzomib, a highly efficient and potent compound, ranked 10th in terms of chronic toxicity, and already showed a very broad therapeutic window with the ratio of adverse to therapeutic effect being 578-fold at day 3. The proteasome inhibitor Carfilzomib as well was a prominent compound within the ranking for SKOV/NIH microtissues (Table S6). This particular compound appeared to be effective and potent, had a significant influence on tumor growth over time and showed a minor chronic toxicity to fibroblasts. In addition, the therapeutic window with the ratio of adverse to therapeutic effect being 1,270 at day 3 was very broad. Another compound, which was outstanding already in the HEY/NIH classification, is Dasatinib. The potent Bcr-Abl inhibitor seems to target very specifically the cancer cells and ranked 13th in terms of efficacy with a max response of 4.244. Another interesting compound was the EGFR inhibitor AV-412, which is listed in all categories, except for the effect on tumor size over time, where it was ranked 11th out of 20. Five compounds may be found within the ranking for PANC/NIH spheroids, shown in Table S4. These are Torin-2, Ponatinib, TAE-684, Carfilzomib and Bardoxolone methyl. The highly potent and efficient mTORC1 inhibitor Torin-2 is listed in all categories, except for efficacy and acute toxicity, where it showed nevertheless a very broad therapeutic window with the ratio of adverse to therapeutic effect being 5,524-fold. It ranked 11th in terms of efficacy with a max response of 3 uM. Bardoxolone methyl, a compound with a high efficacy and an infinite therapeutic window for both acute and chronic toxicity, showed a medium potency

with an IC_{50} value of 1 μM. Figure 6 shows the doses responses for TAK-733 and Dasatinib, two of the compounds which show overall best potency, efficacy and therapeutic window.

DISCUSSION

The effectiveness of a drug in clinic by their therapeutic window in which efficacy is achieved within a manageable framework of toxic adverse effects. Here, by integrating a cytotoxicity readout as an additional parameter in a screening set up, we can define a ranking of compounds with the highest efficacy towards cancer cells with the lowest cytotoxicity towards stromal cells representing unwanted side effects.

The 3D heterotypic multicellular tumor spheroid NanoLUC systems were developed in a 96-well format but are scalable to a 384-well high throughput assay platform which allows to test compounds in dose responses to obtain both efficacy and potency measures over time using different relevant assay readouts of cell viability, size-based growth kinetics and stromal cell viability. Comparison of % maximal responses and AC_{50} values of treated ovarian homotypic with those of ovarian heterotypic microtissues did show minimal differences of drug efficacies and potencies between the two systems. The addition of stromal cells to the formation of heterotypic tumor microtissues, with the resulting heterotypic cell-cell crosstalk, is expected to increase drug resistance of the cancer cells compared to homotypic microtissues [22]. The evaluation of the treatment data did reveal that heterotypic microtissues show a decrease in sensitivity to compounds compared with homotypic microtissues. The differences however were minor, which suggested that additional cell types have minimal influences on drug sensitivity. A finding has been the fact that some of the drugs which showed high effects in potency or efficacy based on intra-tissue ATP contents after 7 days had moderate effects on tissue size development over time. Vice versa, some of the drugs which showed a moderate potency and/or efficacy had a very high influence on tumor growth over time. There was no obvious pattern, if any, which would have shown an unambiguous relationship between these variables.

To model a therapeutic window, which is defined as the ratio adverse effect / therapeutic effect, AC_{50} values based on NanoLUC data were set in relation to AC_{50} values based on ATP data at the day 7 treatment. By tracking NanoLUC data over time, a time-related development of the effects on stromal cells in all microtissue models was detected for compounds which showed medium to high potencies based on ATP data. Taking into account pharmaco- and toxicokinetic aspects, two different therapeutic windows were modeled. NanoLUC data at day 3 represented acute toxicity of the compounds, whereas NanoLUC data at day 7 represented chronic toxicity. The therapeutic window classification in terms of acute toxicity revealed that all the top ten compounds had to be considered as having an infinite therapeutic window. This means that for these compounds no significant effect on the fibroblasts has been verified in reference to the vehicle control. In general, only few compounds did have a toxic effect on the fibroblasts after 3 days of treatment. In contrast to that, the therapeutic window narrowed for most compounds due to chronic toxicity after 7 days of continuous treatment. Therefore, compounds which were listed within the top ten compounds after 3 days of treatment did not show up anymore within the top ten classification for chronic toxicity. Nevertheless, there are some compounds, for

example TAK-733, Dasatinib and Torin-2, which showed a broad therapeutic window even after 7 days of treatment which indicates for very specific targeting of the cancer cells. However, a high target selectivity does not imply necessarily a good clinical safety profile for a drug [23]. The question remains which endpoint is the more relevant to be considered for a transition into clinical testing and how to best mimic dosing schedules. It has been shown that a continuous dosing over 7 days does not comply with the clinical dosing regimens. Romidepsin for example was administered every 28 days on days 1 and 15 in a clinical phase II with pancreatic cancer patients [24]. The recommended dosing schedule for Carfilzomib was set to intravenous infusions of 2–10-min twice a week [25]. However, to determine the optimal dosing of targeted therapy is challenging [26]. It has been currently discussed whether higher drug doses with short exposure times, or longer exposure times with lower doses are beneficial [27]. The fact is that a continuous 7-day treatment does not reflect the in vivo procedure and it is very likely that a temporal dosing in vitro would not affect the fibroblasts as severely as a continuous treatment. In addition, since cancer is a heterogeneous disease and tumor growth does not depend on one single target, future treatment strategies will be based on a combination of different therapies targeting the hallmarks of cancer.

Supplementary Material

Refer to Web version on PubMed Central for supplementary material.

Acknowledgements

We thank the R&D team of InSphero for supporting the work, Promega, Madison for providing the NanoLUC expression cassette and Lonza, Cologne for the 4D-NucleofectorTM transfection unit. Work at NCATS was funded by the NIH Intramural Research Program.

References

1. Waring MJ; Arrowsmith J; Leach AR; et al. An Analysis of the Attrition of Drug Candidates from Four Major Pharmaceutical Companies. Nat. Rev. Drug Discov. 2015, 14, 475. [PubMed: 26091267]
2. Mullard A Industry R&D Returns Slip. Nat. Rev. Drug Discov. 2015, 15, 7.
3. Takimoto CH Anticancer Drug Development at the US National Cancer Institute. Cancer Chemother. Pharmacol. 2003, 52 Suppl 1, S29–33. [PubMed: 12819935]
4. Herrmann R; Fayad W; Schwarz S; et al. Screening for Compounds That Induce Apoptosis of Cancer Cells Grown as Multicellular Spheroids. J. Biomol. Screen. 2007, 13, 1–8. [PubMed: 18040052]
5. Hickman JA; Graeser R; de Hoogt R; et al. Three-Dimensional Models of Cancer for Pharmacology and Cancer Cell Biology: Capturing Tumor Complexity in Vitro/Ex Vivo. Biotechnol. J. 2014, 9, 1115–1128. [PubMed: 25174503]
6. Carragher N; Piccinini F; Tesei A; et al. Concerns, Challenges and Promises of High-Content Analysis of 3D Cellular Models. Nat. Rev. Drug Discov. 2018.
7. Yamada KM; Cukierman E Modeling Tissue Morphogenesis and Cancer in 3D. Cell 2007, 130, 601–610. [PubMed: 17719539]
8. Xu H; Lyu X; Yi M; et al. Organoid Technology and Applications in Cancer Research. J. Hematol. Oncol. 2018, 11, 116. [PubMed: 30219074]

9. Kelm JM; Lal-Nag M; Sittampalam GS; et al. Translational in Vitro Research: Integrating 3D Drug Discovery and Development Processes into the Drug Development Pipeline. Drug Discov. Today 2018.
10. Anton D; Burckel H; Josset E; et al. Three-Dimensional Cell Culture: A Breakthrough in Vivo. International Journal of Molecular Sciences, 2015, 16. [PubMed: 26712738]
11. Ivascu A; Kubbies M Rapid Generation of Single-Tumor Spheroids for High-Throughput Cell Function and Toxicity Analysis. J. Biomol. Screen. 2006, 11, 922–932. [PubMed: 16973921]
12. He J; Xiong L; Li Q; et al. 3D Modeling of Cancer Stem Cell Niche. Oncotarget 2018, 9, 1326–1345. [PubMed: 29416698]
13. Weiswald L-B; Bellet D; Dangles-Marie V Spherical Cancer Models in Tumor Biology. Neoplasia 2015, 17, 1–15. [PubMed: 25622895]
14. Weigelt B; Ghajar CM; Bissell MJ The Need for Complex 3D Culture Models to Unravel Novel Pathways and Identify Accurate Biomarkers in Breast Cancer. Advanced Drug Delivery Reviews, 2014, 69–70. [PubMed: 25451857]
15. Ravi M; Paramesh V; Kaviya SR; et al. 3D Cell Culture Systems: Advantages and Applications. J. Cell. Physiol. 2015, 230.
16. Rimann M; Graf-Hausner U Synthetic 3D Multicellular Systems for Drug Development. Curr. Opin. Biotechnol. 2012, 23, 803–809. [PubMed: 22326911]
17. Halfter K; Ditsch N; Kolberg H-C; et al. Prospective Cohort Study Using the Breast Cancer Spheroid Model as a Predictor for Response to Neoadjuvant Therapy – the SpheroNEO Study. BMC Cancer 2015, 15, 519. [PubMed: 26169261]
18. Jenkins RW; Aref AR; Lizotte PH; et al. Ex Vivo Profiling of PD-1 Blockade Using Organotypic Tumor Spheroids. Cancer Discov. 2018, 8, 196–215. [PubMed: 29101162]
19. Froeling FEM; Marshall JF; Kocher HM Pancreatic Cancer Organotypic Cultures. J. Biotechnol. 2010, 148, 16–23. [PubMed: 20083148]
20. Hanahan D; Weinberg RA Hallmarks of Cancer: The Next Generation. Cell 2011, 144, 646–674. [PubMed: 21376230]
21. Shield K; Ackland ML; Ahmed N; et al. Multicellular Spheroids in Ovarian Cancer Metastases: Biology and Pathology. Gynecol. Oncol. 2009, 113, 143–148. [PubMed: 19135710]
22. Zhang W; Huang P Cancer-Stromal Interactions. Cancer Biol. Ther. 2011, 11, 150–156. [PubMed: 21191189]
23. Muller PY; Milton MN The Determination and Interpretation of the Therapeutic Index in Drug Development. Nat. Rev. Drug Discov. 2012, 11, 751–761. [PubMed: 22935759]
24. Jones SF; Infante JR; Spigel DR; et al. Phase 1 Results from a Study of Romidepsin in Combination with Gemcitabine in Patients with Advanced Solid Tumors. Cancer Invest. 2012, 30, 481–6. [PubMed: 22536933]
25. Papadopoulos KP; Burris HA; Gordon M; et al. A Phase I/II Study of Carfilzomib 2–10-Min Infusion in Patients with Advanced Solid Tumors. Cancer Chemother. Pharmacol. 2013, 72, 861–868. [PubMed: 23975329]
26. Gerber DE Targeted Therapies: A New Generation of Cancer Treatments. Am. Fam. Physician 2008, 77, 311–9. [PubMed: 18297955]
27. Jokinen E; Koivunen JP MEK and PI3K Inhibition in Solid Tumors: Rationale and Evidence to Date. Ther. Adv. Med. Oncol. 2015, 7, 170–180. [PubMed: 26673580]

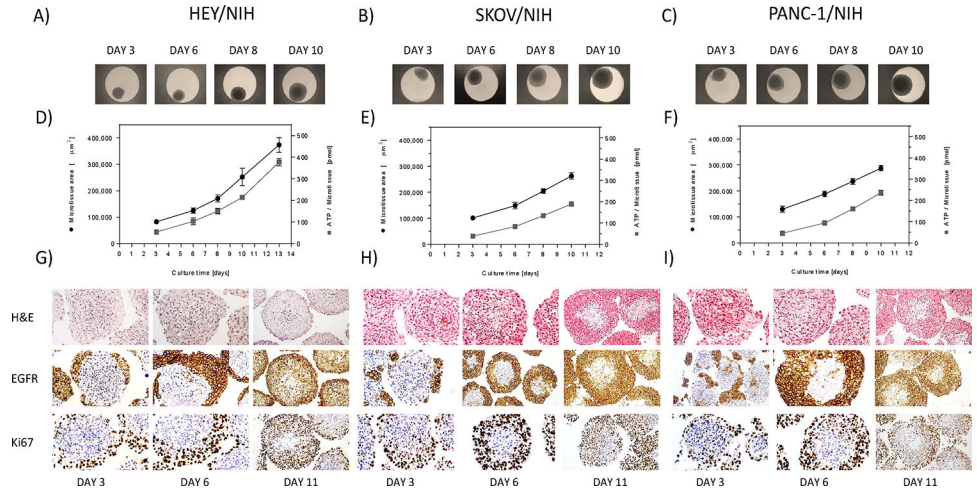

Figure 1.

Growth profiles and morphological appearance 3D heterotypic multicellular tumor spheroids. A-C) Co-culture spheroids of HEY, SKOV-3 and PANC-1 cancer cells and NIH3T3 fibroblasts were produced with the hanging drop technology and their growth monitored over time by bright field microscopy. D-F) After 3 days of spheroid formation, tissue size (●) and intra-tissue ATP content (■) were monitored over 7 days. Each point represents the mean of 8 spheroids and their corresponding standard deviation. Bright field microscopy allowed for size assessment of the microtissues and intra-tissue ATP with CellTiterGlo™ was used as a measure of cell viability. G-I) All three heterotypic tumor microtissues were stained for histological characterization. Cancer and stromal cells were capable of reforming heterotypic, solid spheroids, as shown by hematoxylin and eosin staining. Eosin colors eosinophilic structures in various shades of red, pink and orange, whereas hematoxylin colors nuclei of cells blue. After 11 days of culture, tumor microtissues formed a necrotic area in the center of the spheres, composed of cells undergoing apoptosis and or necrosis, most likely due to hypoxia. The spheroids showed a high expression of EGRF within the cancer cells. Heterotypic tumor spheroids exhibited a spherical geometry with a central core of non-proliferating fibroblasts and proliferating cancer cells in the periphery. Differences of the individual cell types could be clearly displayed by IHC staining of Ki67.

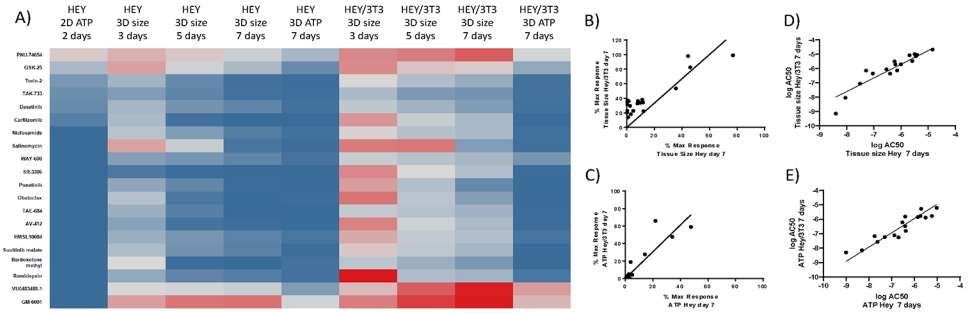

Figure 2.

Comparison of pharmacological effects of compounds on HEY cancer growth assays of increased complexity, as measured by cell viability with CellTiterGlo™ and spheroid size by bright field microscopy. A) The heat map illustrates % maximal responses at 40 μM (2D) and 20 μM (3D) drug concentrations, calculated based on ATP data for 2D, 3D HEY and 3D HEY/NIH cultures, as well as size measurements from 3D microtissues of HEY and HEY/NIH over time. Darkest red indicates 100 % viability for ATP data, respectively 100 % growth for tissue size data. Darkest blue indicates 0 % viability for ATP data, respectively 0 % growth for tissue size data. For % maximal response calculations, ATP and tissue size values were normalized to the vehicle control. Correlation plots of % maximal response (B, C) and $\log AC_{50}$ (D,E) between homo- and heterotypic HEY microtissues. Straight line corresponds to a liner fit to the data.

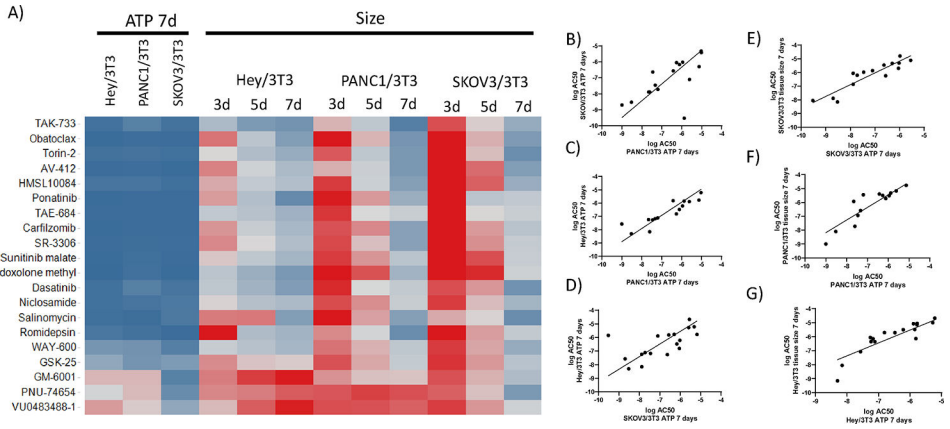

Figure 3.

Comparison of pharmacological effects of compounds on 3D heterotypic multicellular tumor spheroids of different cancer types. A) The heat map illustrates size-based % maximal responses at 20 μM drug concentrations calculated over time from HEY/NIH, PANC/NIH and SKOV/NIH microtissues. Darkest red indicates 100 % growth for tissue size data. Darkest blue indicates 0 % growth for tissue size data. For % maximal response calculations tissue size values were normalized to the vehicle control. Correlation plots of $\log AC_{50}$ between different tumor microtissue types using ATP 7 days as a readout (B-D), and between ATP and tissue size at 7 days, for each cancer microtissues (E-G).

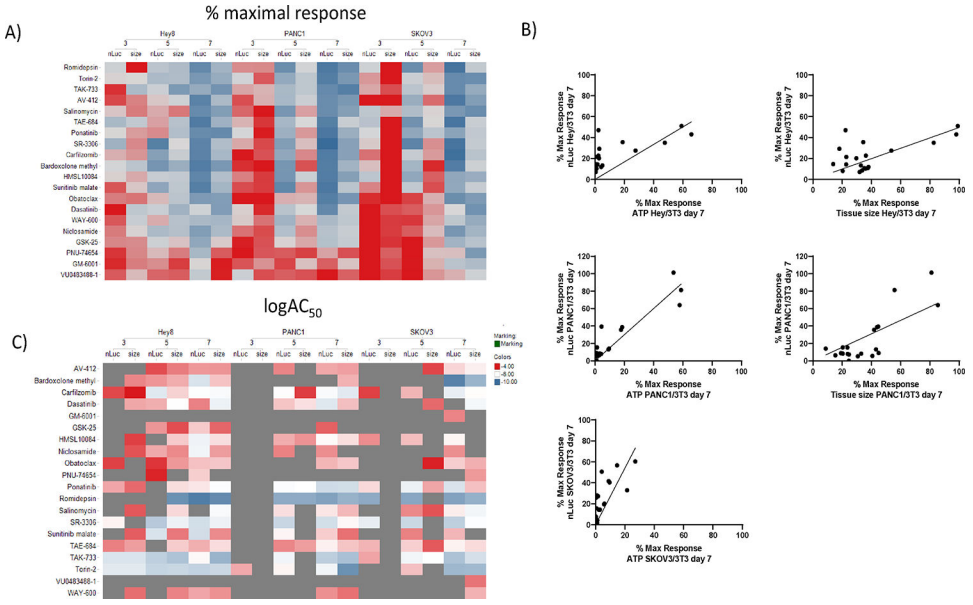

Figure 4.

Comparison of pharmacological effects of compounds on NanoLUC reporter from fibroblasts cells and spheroid size on 3D heterotypic multicellular tumor spheroids of different cancer types. A) The heat map illustrates % maximal responses at 20 μM drug concentrations calculated based on tissue size and NanoLUC luminescence measurements over time for HEY/NIH, PANC/NIH and SKOV/NIH microtissues. Darkest red for tissue size indicates 100 % size of the entire microtissue, and for NanoLUC data it indicates 100 % viability of the fibroblasts within the microtissue. Darkest blue for tissue size data indicates 0 % tissue and for NanoLUC data it indicates 0 % viability of the fibroblasts within the microtissue. B) Correlation plots of % maximal responses between NanoLuc and tissue size readouts in the same cancer tissues, and the same readouts across different cancer microtissues. C) Heat map a heat map comparing the $logAC_{50}$ values calculated from doses responses based on tissue size and NanoLUC luminescence measurements over time for HEY/NIH, PANC/NIH and SKOV/NIH microtissues. Those conditions for which a compound had no efficacy and IC_{50} could be calculated are indicated in grey.

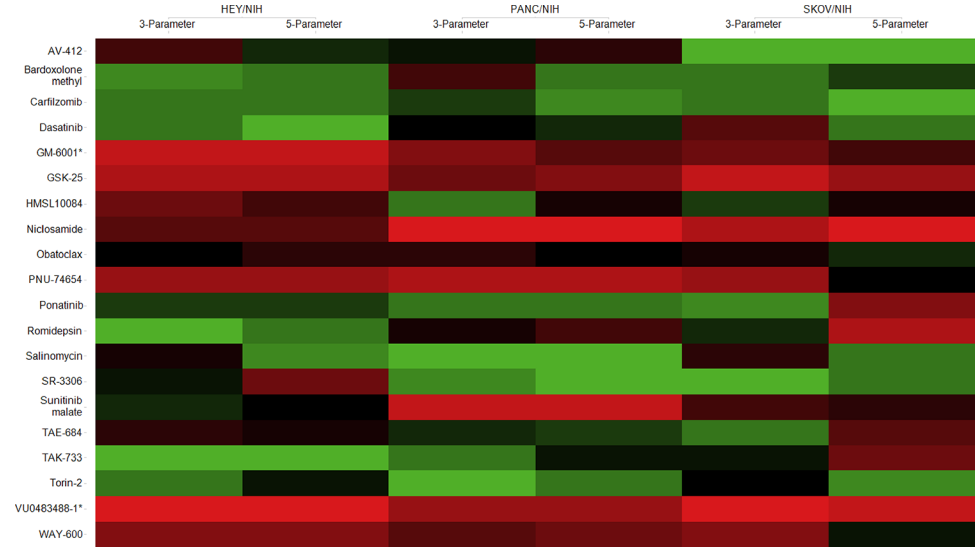

Figure 5.

Heat map based on rank changes of the individual compounds between 3- and 5-parameter classifications. Colored by ranking score: 1 (green) corresponds to the best therapeutic window, and 20 (red) corresponds to the smallest therapeutic window.

Table 1.

Therapeutic Windows, as the Ratio of Adverse Effect to Therapeutic Effect, for 3-Day and 7-Day Cytotoxicity of the Compounds in HEY/NIH, SKOV/NIH, and PANC1/NIH Spheroids.

Compound name	HEY/NIH			SKOV/NIH			PANC/NIH				
	IC_{50} ATP (μM)	Therapeutic window		IC_{50} ATP (μM)	Therapeutic window		IC_{50} ATP (μM)	Therapeutic window		Hallmark categorization	Primary target
		3-day TOX	7-day TOX		3-day TOX	7-day TOX		3-day TOX	7-day TOX		
HMSL10084	0.333	*infinite	1.396	0.683	14.7	1.817	0.767	*infinite	1.443	*SustProlifSign	FLT3
AV-412	1.292	*infinite	6.026	0.08	*infinite	28.42	2.444	*infinite	2.338	*SustProlifSign	EGFR
TAK-733	0.007	25.57	161.600	0.013	467.6	1.692	0.025	*infinite	1.800	*SustProlifSign	MEK
SR-3306	0.058	21.77	2 138	0.013	24.85	3.692	0.022	*infinite	5.636	*SustProlifSign	JNK 1/2/3
TAE-684	0.155	81.68	31.960	0.905	4.966	1.439	0.548	*infinite	2.473	*SustProlifSign	ALK
Cantharidin	3.168	*infinite	1.045							*SustProlifSign	PP-1;PP-2A
Dasatinib	0.077	*infinite	158.700	0.019	*infinite	*infinite	0.064	*infinite	3.578	*ResistCellDeath	Bcr-Abl
VU0483488-1				1.042	*infinite	*infinite	*n.d.	*n.d.	*n.d.	*ResistCellDeath	McI-Inh
Obatoclax	0.609	71.19	5,619.000	0.959	*infinite	2.773	1.110	*infinite	3.878	*ResistCellDeath	Bcl-xL
Niclosamide	1.668	*infinite	0.329	6.649	*infinite	1.404	*n.d.	*n.d.	*n.d.	*ResistCellDeath	STAT-3
PD-173955	0.479	*infinite	20.370							*ResistCellDeath	cSRC
Sepantronium bromide	0.279	*infinite	55.190							*ResistCellDeath	Suivivin
PNU-74654	21.160	*infinite	0.126	2.835	*infinite	*infinite	*n.d.	*n.d.	*n.d.	*StPS/RCD	Wnt Signaling
WAY-600	1.681	*infinite	3.486	0.507	*infinite	*infinite	7.377	*infinite	1.240	*StPS/RCD	mTOR
Torin-2	0.027	9.629	2.222	0.002	*infinite	6.000	0.001	5 524	540	*StPS/RCD	mTORC1
Romidepsin	0.005	*infinite	0.060	0.003	1,667	1.000	0.003	*infinite	1	*StPS/RCD	HDAC
Carfilzomib	0.067	577.8	12.850	0.035	1 270	10.14	0.047	*infinite	15,47	*StPS/RCD	Proteasome
Bardoxolone methyl	1.414	*infinite	0.120	0	*infinite	1.333	1.335	*infinite	*infinite	*StPS/RCD	NF-kappaB
Cycloheximide	0.022	395.91	51.860							*StPS/RCD	GSK-3beta
GSK-25	6.099	*infinite	0.473	4.829	*infinite	*infinite	9.375	*infinite	2.466	*activInvasMetast	ROCK
GM-6001				3.856	*infinite	3.006	9.614	*infinite	*infinite	*activInvasMetast	MMP Inh
Ponatinib	0.055	106.2	29.710	0.233	9.219	0.755	0.035	*infinite	2.971	*induceAngio	FGFR

SLAS Discov. Author manuscript; available in PMC 2024 July 25.

Compound name	HEY/NIH			SKOV/NIH			PANC/NIH				
	IC_{50} ATP (μM)	Therapeutic window		IC_{50} ATP (μM)	Therapeutic window		IC_{50} ATP (μM)	Therapeutic window		Hallmark categorization	Primary target
		3-day TOX	7-day TOX		3-day TOX	7-day TOX		3-day TOX	7-day TOX		
Sunitinib malate	5.270	*infinite	0.023	2.595	*infinite	1.642	*n.d.	*n.d.	*n.d.	*induceAngio	VEGFR
HLI-373989	3.755	*infinite	1.188							*evadGrowthSign	MDM2
DA-3003-1	7.359	*infinite	*infinite							*evadGrowthSign	CDC25
Topotecan hydrochloride	0.025	*infinite	2.960							*trad.chemo.	DNA Topoisomerase I
Salinomycin	1.530	*infinite	*infinite	0.274	*infinite	5.274	0.377	*infinite	4.401	*n.c.	Anticoccidial/ Antibact.
Amiodarone	56.460	*infinite	*infinite							*n.c.	Muscarinic M3 Recept.
Benzamil	113.500	*infinite	*infinite							*n.c.	Epithel. Sodium Chan.
SK&F-89976A	15.280	*infinite	*infinite							*n.c.	GAT-1
G-Strophanthin	0.070	*infinite	1.433							*n.c.	Na+/K+-ATPase
Digoxin	0.107	*infinite	0.449							*n.c.	Steroid
Shikonin	5.954	*infinite	1.607							*n.c.	Chemokine receptors

SLAS Discov. Author manuscript; available in PMC 2024 July 25.